

Article

The Effect of the Thickness of the Sensitive Layer on the Performance of the Accumulating NO_x Sensor

Andrea Groß¹, Miriam Richter¹, David J. Kubinski², Jacobus H. Visser² and Ralf Moos^{1,*}

¹ University of Bayreuth, Zentrum für Energietechnik, Lehrstuhl für Funktionsmaterialien, Bayreuth 95440, Germany

² Ford Research and Advanced Engineering, Dearborn, MI 48124, USA

* Author to whom correspondence should be addressed;

E-Mail: Functional.Materials@uni-bayreuth.de; Tel.: +49-921-55-7401; Fax: +49-921-55-7405.

Received: 2 August 2012; in revised form: 28 August 2012 / Accepted: 31 August 2012 /

Published: 10 September 2012

Abstract: A novel and promising method to measure low levels of NO_x utilizes the accumulating sensor principle. During an integration cycle, incoming NO_x molecules are stored in a sensitive layer based on an automotive lean NO_x trap (LNT) material that changes its electrical resistivity proportional to the amount of stored NO_x, making the sensor suitable for long-term detection of low levels of NO_x. In this study, the influence of the thickness of the sensitive layer, prepared by multiple screen-printing, is investigated. All samples show good accumulating sensing properties for both NO and NO₂. In accordance to a simplified model, the base resistance of the sensitive layer and the sensitivity to NO_x decrease with increasing thickness. Contrarily, the sensor response time increases. The linear measurement range of all samples ends at a sensor response of about 30% resulting in an increase of the linearly detectable amount with the thickness. Hence, the variation of the thickness of the sensitive layer is a powerful tool to adapt the linear measurement range (proportional to the thickness) as well as the sensitivity (proportional to the inverse thickness) to the application requirements. Calculations combining the sensor model with the measurement results indicate that for operation in the linear range, about 3% of the LNT material is converted to nitrate.

Keywords: lean NO_x trap (LNT); NO_x storage and reduction catalyst (NSR); low ppm-level NO_x sensing; semiconducting gas sensor; linear measurement range adaption; carbonate nitrate conversion

1. Introduction

Tightened emission and safety regulations have increased the demand for sensitive devices to detect reliably even low levels of NO and NO₂ (NO_x) over a long measurement period [1–3] (e.g., summarized as <100 ppm NO_x in the automotive exhaust and 0.5–5 ppm NO₂ in the interior by [1]). In the field of automotive or industrial exhausts or of air quality management, the interest is on the accurate determination of mean values (e.g., 1-h value for air quality monitoring [4]) or total amounts (e.g., cumulated vehicle emissions in g/km for on-board diagnostics [5,6]) rather than on the curve of the actual instantaneous concentration over time. However, most today's gas sensors measure time-continuously the actual analyte concentration [1]. Cumulated amount mean values are obtained by mathematical averaging (integration). Due to inaccuracies at low analyte levels, long sensor response times and recovery times, as well as due to drifts in the zero point level (baseline), these sensors are subject to errors in the determination of the accumulated analyte levels [2,3,7].

Alternatively the accumulating-type (or integrating-type or dosimeter-type) sensor measures directly the total amounts of analyte gases over a time interval. This novel principle is related to passive samplers being used to determine the cumulated analyte level in two steps. There, over a longer period (e.g., a month) analyte molecules from the ambience are collected in a diffusion controlled process on a sorption material, followed by a quantitative analysis with laboratory gas analysis methods [8,9]. Accumulating-type gas sensors presented here are also based on a sensitive layer that collects analyte molecules over a longer period, but in contrast to passive samplers, the analyte level is evaluated instantaneously and time-continuously by electrical means. While chemically sorbing the analyte molecules, the electrical properties of the sensitive layer, e.g., the resistivity, change with the amount of analyte stored. Like in passive samplers, the sorbent material needs to be regenerated periodically as saturation effects occur. The sensor signal of the accumulating NO_x sensor correlates directly with the total amount of NO_x (being the sum of NO and NO₂), whereas the curve of the actual concentration can be obtained from the timely derivative of the sensor signal [10]. By collecting analyte molecules from the gas stream, even small levels contribute to the sensor signal, enabling accurate analyte detection over an extended time interval. Another important feature is the fact that errors in the sensor's zero level are minimized since the zero-level is redefined after each regeneration step. Both response times and recovery times of the signal derivative as the measurand for the actual concentration are quite low and in the range of the gas exchange time of the setup (<7 s [10]). The fast sensing characteristics of the accumulating sensor originate from the fact that the change (*i.e.*, the time-based derivative) in the conductivity during NO_x exposure correlates with the NO_x concentration. This is in strong contrast to common gas sensors, in which the equilibrium conductivity of the sensor signal is of interest. In the following, the effect of the thickness of the NO_x storage layer on the NO_x accumulating sensing properties is addressed.

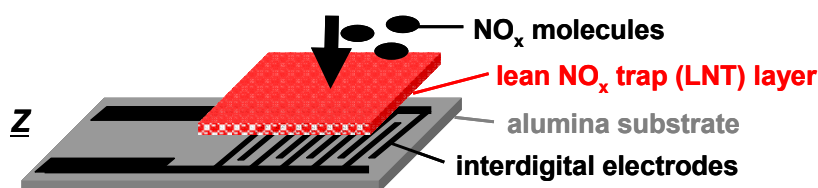
2. The Accumulating Sensing Concept

The accumulating or integrating-type sensor is intended to detect directly the total amount, A , of low levels of analyte by accumulation. Generally, A can be calculated according to Equation (1) from the analyte concentration, $c(t)$, and the flow rate, $\dot{V}(t)$. Both may vary with time.

$$A = \int c(t) \cdot \dot{V}(t) dt \quad (1)$$

In [11] two setups of the integrating NO_x sensor are presented. Utilizing a special channel-type setup with a large area of sensitive material compared to the small gas volume inside the channel, all analyte molecules become sorbed and the resulting sensor signal reflects the total amount, A , even if the flow rate of the gas varies (amount detector). Contrarily, it was investigated in [11] that by exposing the sensitive layer of the planar device to a large gas volume, always a constant fraction of the analyte molecules in the gas stream is stored independently on the gas flow rate in a wide range. The sensor signal correlates then with the timely integral of the concentration, $\int c(t) dt$. If the flow rate, $\dot{V}(t)$, remains constant, A is directly proportional to the integral of $c(t)$, *i.e.*, $A \propto \int c(t) dt$ and the total amount can be determined properly with the planar setup while the signal derivative reflects the curve of $c(t)$ [10].

Figure 1. Planar sensor setup of the impedimetric accumulating NO_x sensor based on a lean NO_x trap layer deposited on interdigital electrodes.



For the accumulating sensing principle sensitive layers of storage materials can be applied. They are able to sorb analyte molecules (e.g., by chemisorption or by a chemical reaction) and thereby they change their electrical properties. As illustrated in Figure 1, the accumulating NO_x sensor in the planar setup (concentration integrator) consists of a lean NO_x trap (LNT) layer deposited on an alumina substrate which is equipped with interdigital electrodes (IDEs). It is well known that LNT materials lower their resistivity when transformed from carbonates to nitrates upon NO_x storage [12–15]. Since the accessible sorption sites in the storage material are becoming occupied with proceeding sorption, saturation effects limit the accumulating properties and a regeneration of the sorption sites is required to recover the original sorption capacity. Therefore, as illustrated in Figure 2(a), in the operation of accumulating sensors the sensing interval during which the sensitive layer (shaded area) accumulates the analyte molecules (black points) from the gas stream alternates with the regeneration interval. The absolute value of the relative resistance change, R_{rel} , calculated by Equation (2) with R_0 being the base resistance in the unloaded state, is displayed as the accumulating NO_x sensor signal:

$$R_{\text{rel}} = \frac{|\Delta R|}{R_0} = \frac{R_0 - R}{R_0} \quad (2)$$

R_{rel} depends on the loading level which, for low loading states, is proportional to the amount of NO_x in the gas phase, A , as illustrated in Figure 2(b). The sensor signal on the time scale differs from those of conventional gas sensors due to the stepwise NO_x accumulation. As shown in Figure 2(c), R_{rel} (black line) increases in the presence of NO_x , whereas it remains constant in the NO_x absence (holding ability)— R_{rel} is proportional to A (dark grey line, dotted). In the case of a constant flow rate, $\dot{V}(t)$, the timely increase of the sensor signal is proportional to the NO_x concentration c (light grey line, right axis). This proportionality enables to determine the curve of the instantaneous concentration using the timely derivative, dR_{rel}/dt . In the following, dR_{rel}/dt will be denoted as \dot{R}_{rel} :

$$\dot{R}_{\text{rel}} = \frac{dR_{\text{rel}}}{dt} \quad (3)$$

\dot{R}_{rel} is illustrated as a function of time in Figure 2(d). As depicted in Figure 2(e), there is a linear correlation between \dot{R}_{rel} and c . Hence, to compare the performance of the accumulating sensor with conventional gas sensors, the characteristics of \dot{R}_{rel} are appropriate. The sensitivity is commonly defined as the slope of the characteristic line which is the correlation between the sensor signal and the measurand [16]. Hence, for the accumulating type NO_x sensor, which is intended to determine A , the amount sensitivity, S_A , (Figure 2(b)) can be calculated from the correlation between R_{rel} and A according to Equation (4) resulting in the unit $\%/\mu\text{L}$. Additionally, in the case of a constant flow rate, the proportionality between \dot{R}_{rel} and c , as shown in Figure 2(e), allows to calculate the concentration sensitivity, S_c , according to Equation (5) which is analogous to the sensitivity known of conventional gas sensors:

$$S_A = \frac{dR_{\text{rel}}}{dA} \quad (4)$$

$$S_c = \frac{d(dR_{\text{rel}}/dt)}{dc} = \frac{d\dot{R}_{\text{rel}}}{dc} \quad (5)$$

If one transforms Equation (4) using Equation (1), one obtains:

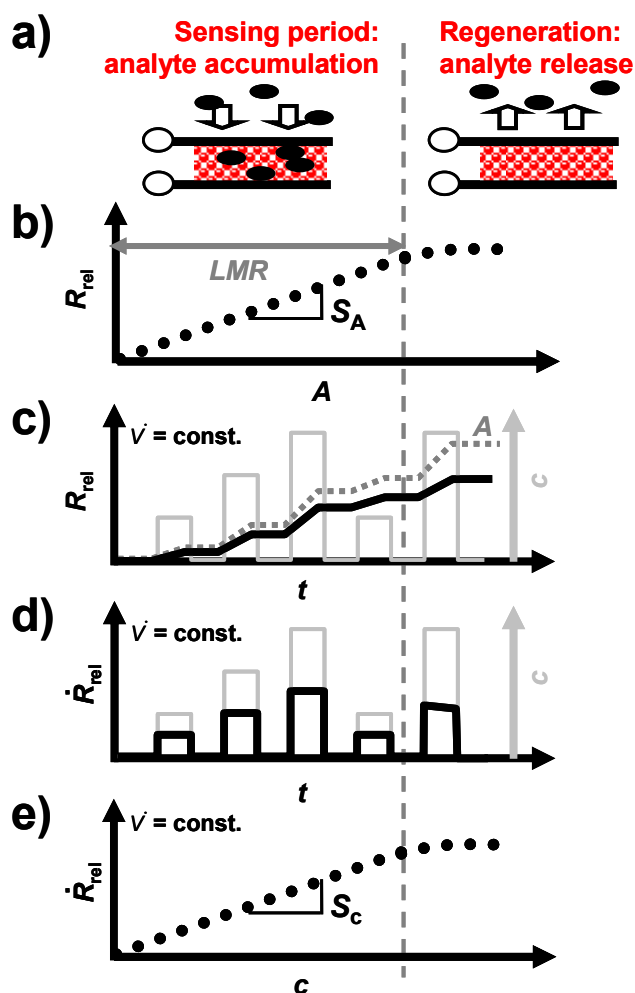
$$S_A = \frac{dR_{\text{rel}}}{dA} = \frac{dR_{\text{rel}}/dt}{dA/dt} = \frac{\dot{R}_{\text{rel}}}{d(\int c(t) \cdot \dot{V}(t) dt)/dt} = \frac{\dot{R}_{\text{rel}}}{\dot{V} \cdot c} \quad (6)$$

If $S_c = \text{const}$, *i.e.*, $\dot{R}_{\text{rel}} \propto c$, then $d\dot{R}_{\text{rel}}/dc$ can be replaced by \dot{R}_{rel}/c . Then the relation between S_c and S_A yields:

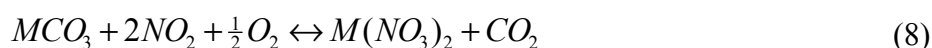
$$S_A = \frac{1}{\dot{V}} S_c \quad (7)$$

In other words, the amount-related sensitivity, S_A , and the “classical” sensitivity with respect to the concentration, S_c , are proportional to each other, as long as the gas flow remains constant. As shown in Figure 2(b,e), as soon as saturation effects occur and the linear measurement range, LMR , is exceeded, S_A and S_c decrease, and the slope of the signal no longer reflects the concentration (Figure 2(b–e))—the accumulating sensor demands regeneration.

Figure 2. Scheme of the accumulating sensing principle: (a) Operation with alternating sensing and regeneration periods; (b) characteristic line to determine the total amount: linear correlation between the sensor response and the amount A in the linear measurement range, LMR ; (c) sensor signal on the time scale, R_{rel} (black full line), increases in the presence of NO_x ; amount A (dotted grey line) calculated acc. to Equation (1); (d) signal derivative \dot{R}_{rel} reflects the actual concentration c ; (e) correlation between \dot{R}_{rel} and c .



LNT materials are known from automotive NO_x storage and reduction catalysts to reduce the NO_x emissions in the exhaust [17–19]. Since NO_x molecules can be stored in a lean gas atmosphere, whereas they are released and reduced in rich gas compositions, the engine operation cycles between long lean and short rich intervals to ensure low emissions [5,17–19]. LNTs usually consist of alkaline (earth-) oxides or carbonates (e.g., $BaCO_3$ or K_2CO_3) as storage components, finely dispersed precious metal particles to catalyze oxidation and reduction reactions, and support oxides like Al_2O_3 to provide high surface areas for the catalytic processes [19,20]. The storage mechanism is based on the conversion of alkaline (earth-) carbonates MCO_3 or oxides to nitrates $M(NO_3)_2$ upon NO_2 exposure according to Equation (8). NO needs to be oxidized to NO_2 on the catalytic active particles prior to the nitrate formation according to Equation (9) [17,18,20]:





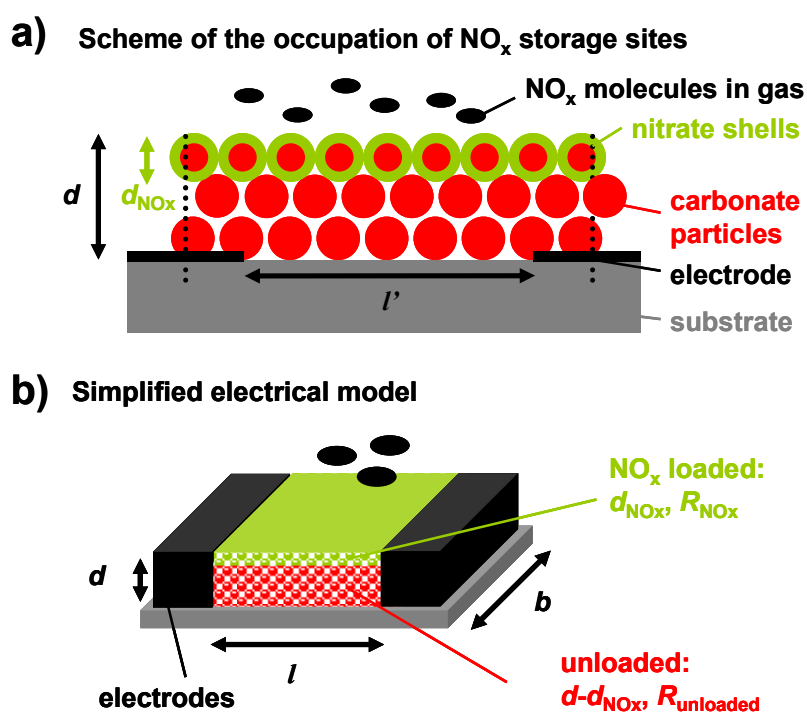
We recently demonstrated the integrating or accumulating NO_x sensing principle under various gas conditions (base gas composition, temperature) [10,21,22]. Additionally, it was found that the sensitivity to NO is the same as that to NO_2 , thus allowing for total NO_x detection, and that the sensor is suitable for long-term detection of low levels of NO_x [10]. O_2 and CO_2 concentration variations were found to be negligible in a wide range in lean gas containing O_2 , CO_2 and H_2O [10,21].

In order to understand further how NO_x storage occurs in the catalyst material, the influence of the thickness of the sensitive layer on the performance of the accumulating NO_x sensor is the focus of this study. This is motivated by the idea that the number of accessible storage sites and hence the fraction of sites occupied by NO_x upon NO_x exposure should depend on the thickness of the LNT coating if the LNT coated area remains the same. The obtained results may even be of interest for LNT catalyst research and may help to elucidate more details about the storage reactions.

3. Expected Influence of the Thickness of the Sensitive Layer—Some Pre-Considerations

The storage capacity and hence the number of accessible storage sites control the analyte accumulation properties of LNT catalysts. Hence, it is expected that the thickness of the carbonate layer affects the accumulating sensing properties. As described in Figure 3, a simplified model of the configuration containing the storage material (red) and the interdigital electrodes (black) was developed for a rough estimation of this influence.

Figure 3. Model of the influence of the thickness of the sensitive layer on the electrical properties: (a) Mechanism of the storage of NO_x as nitrate shells on carbonate cores at the surface of the NO_x storage layer; (b) simplified electrical model consisting of a parallel circuit of the NO_x loaded material and the remaining unloaded layer.



From catalyst research it has been known that NO_x storage occurs mainly at the surface of the LNT material that is in contact with the gas phase, resulting in less than 40% utilization of the available storage sites upon saturation [23–25]. This means that even in the highly loaded state, only a fraction of the storage sites are involved in the storage process. Additionally, nitrate formation is accompanied by a shrinking of the pore structure since the nitrates have a higher molar volume than the corresponding carbonates [26]. In the case of K_2CO_3 , the volume theoretically increases by almost 70% upon storing NO_x . The decreased diameter of the pores lowers the diffusion of the NO_x molecules into the carbonate particles and the NO_x loaded zones can be modeled as dense nitrate shells at the surface of the LNT particles (shrinking core type model [26,27]). Since the accumulating NO_x sensor is exposed to small NO_x concentrations and is only operated in the low loading state, nitrate shells are expected to form mainly at the upper surface area of the LNT layer, which is in close contact to the analyte gas phase. Hence, the occupation of NO_x storage sites in the sensitive layer by NO_x molecules can be illustrated as shown in Figure 3(a). Thereby, the thickness of the NO_x loaded area, d_{NO_x} , increases with progressive NO_x exposure. If the distance between the electrodes, l' , is much larger than the film thickness, d , the electrical field lines between the electrode fingers are parallel and homogeneously distributed. Almost the entire flux is inside the material [28]. Hence, in a simplified model of the sensor setup, the LNT layer can be described as a resistive material in between two parallel electrodes with the distance l (Figure 3(b)). The term l is related to the distance of the planar electrodes of the IDEs, l' . The relation between l and l' can be calculated which has even been experimentally proven in [29].

Applying this simplified model of Figure 3(b) for the case of the regenerated state ($d_{\text{NO}_x} = 0$), the base resistance of the accumulating NO_x sensor in the unloaded state, R_0 , can be calculated from the geometry and the resistivity of the carbonate material, ρ_0 , by Equation (10). Therefore, it is expected that R_0 correlates with the inverse thickness, $1/d$:

$$R_0 = \rho_0 \frac{l}{bd} \propto \frac{1}{d} \quad (10)$$

Upon exposure to NO_x , it is assumed that surface nitrate is formed. Hence, the corresponding simplified model in the partly loaded state contains a thin nitrate film with the resistance R_{NO_x} and the thickness d_{NO_x} on top of the remaining unloaded material with the resistance R_{unloaded} , as shown in Figure 3(b). The resulting resistance of the sensitive layer, R , can be calculated as a parallel circuit of both fractions ($R_{\text{NO}_x} || R_{\text{unloaded}}$). The sensor signal R_{rel} can then be calculated from the sensor geometry, the resistivity of the sensitive material in the unloaded state, ρ_0 , and the resistivity of the NO_x loaded material, ρ_{NO_x} , according to Equation (11):

$$R_{\text{rel}} = \frac{|\Delta R|}{R_0} = \frac{1}{\frac{d}{d_{\text{NO}_x}(\rho_0/\rho_{\text{NO}_x} - 1)} + 1} \quad (11)$$

d_{NO_x} can be assumed to be very small compared to the thickness of the sensitive layer, d , since only the lightly loaded state is considered. If it is further considered that the resistivity decreases by at least one order of magnitude in the presence of NO_x , Equation (11) can be simplified to Equation (12) meaning that R_{rel} is proportional to $1/d$:

$$R_{\text{rel}} \approx \frac{d_{\text{NO}_x} \cdot (\rho_0 / \rho_{\text{NO}_x} - 1)}{d} \propto \frac{1}{d} \quad (12)$$

Since A is independent of d and the same amount of NO_x is expected to result in the same thickness of the formed NO_x loaded layer, Equations (4) and (12) lead to Equation (13) and the amount-sensitivity, S_A , should correlate with $1/d$ as well:

$$S_A = \frac{dR_{\text{rel}}}{dA} \approx \frac{\rho_0 / \rho_{\text{NO}_x} - 1}{d} \cdot \frac{d(d_{\text{NO}_x})}{dA} \propto \frac{1}{d} \quad (13)$$

As the resistivity decreases by at least one order upon saturation in NO_x , $(\rho_0 / \rho_{\text{NO}_x} - 1) \geq 10$ and Equation (13) can be simplified to Equation (14):

$$S_A = \frac{dR_{\text{rel}}}{dA} \approx \frac{\rho_0}{\rho_{\text{NO}_x}} \cdot \frac{1}{d} \cdot \frac{d(d_{\text{NO}_x})}{dA} \propto \frac{1}{d} \quad (14)$$

Since $S_A \propto S_c$ for constant gas flows, even the classical concentration-related sensitivity, S_c , is expected to depend on $1/d$ and to increase the thinner the sensing layers are.

This simplified model points out that the thickness of the sensitive layer might be an effective tool to vary the sensing properties (especially the sensitivity) of the accumulating NO_x sensor. In the following study, the model was validated by exposing samples with various thicknesses to NO_x containing gas flows and monitoring the sensing performance.

4. Experimental

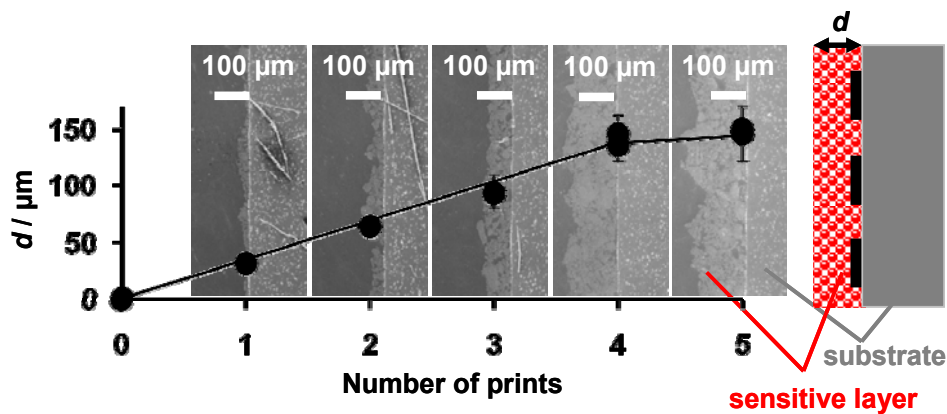
Samples with coatings of different thicknesses were prepared and exposed to various gas compositions containing NO , NO_2 or total NO_x . As illustrated in Figure 1, the accumulating NO_x sensor consists of an LNT layer (potassium-based LNT material provided by Johnson Matthey, composition details given in [30]) deposited on platinum interdigital electrodes (IDEs) with an area of $5 \times 6 \text{ mm}^2$ and an electrode width and spacing of $100 \text{ }\mu\text{m}$ on an alumina substrate with a purity of 96%. After drying and milling the catalyst powder, a screen-printable paste was made by adding organic additives (KD 2721, Zschimmer & Schwarz). To obtain samples with sensitive layers in various thicknesses, the IDE area was screen-printed multiple times with the LNT-paste with intermediate drying periods. After firing at $650 \text{ }^\circ\text{C}$ to remove organic additives, the sensing properties of the samples were analyzed at $380 \text{ }^\circ\text{C}$ in a sensor test bench. Thereby, lean measurements periods and rich desorption periods were periodically applied. The gas flow was kept constant at $\dot{V}(t) = 2 \text{ L/min}$. The base lean gas consisted of 10% O_2 , 5% CO_2 , and 50% N_2 humidified (by a water bubbler at room temperature) in N_2 , whereas the rich gas for regeneration contained 1.5% H_2 , 5% CO_2 , and 50% N_2 humidified in N_2 . Different NO_x gas compositions were admixed. The NO and NO_2 concentrations were monitored by a chemiluminescence detector downstream of the sensor sample. The complex impedances of the sensitive devices were measured in the frequency range from 0.1 Hz to 20 MHz. The electrical characteristics of the bulk material can be described by an $R||C$ parallel equivalent circuit. In time-continuous measurements, R was calculated from the impedance taken at 1 kHz applying the $R||C$ model. The thicknesses of the sensitive layers were estimated using SEM micrographs.

5. Results and Discussion

5.1. Thickness Determination from SEM Analysis

SEM images from the cross sections of the sensor samples printed multiple times with the LNT paste and an illustration for clarification reasons are shown in Figure 4. The microstructure of the sensitive layers is dominated by loose grains of different diameters. The thickness increased with each printing step from about 30 μm (printed only once) to 150 μm (printed five times). The samples printed four and five times had almost the same thickness. This might be due to a densification of the LNT material with successive printing as it is well known when printing porous films or due to an erroneous thickness determination as a result of the increased roughness. In general, the surface is very rough, with an increasing roughness in the case of thicker coatings lowering the accuracy of the thickness evaluation.

Figure 4. SEM analysis to estimate the thickness of the sensitive layers as a function of the number of prints.

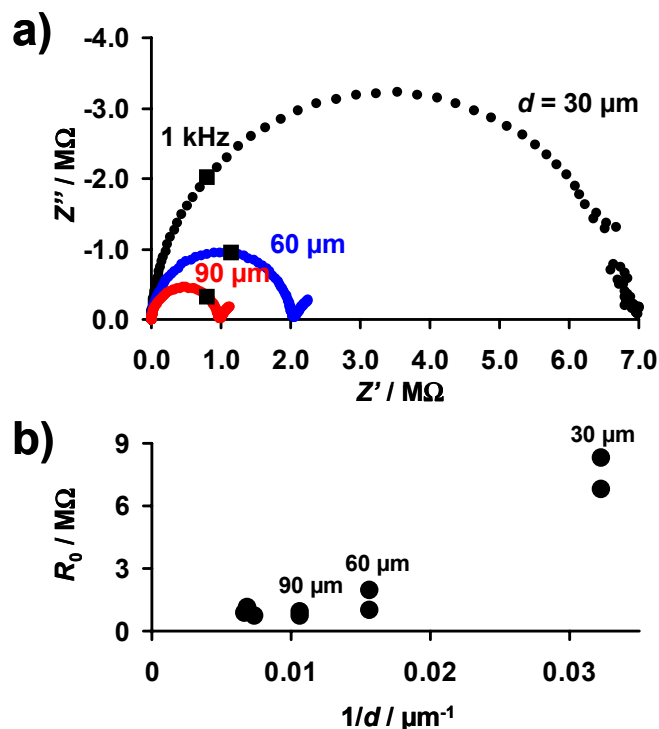


5.2. Base Resistance as a Function of the Thickness

As described above, the base resistance of the sensitive layer in the unloaded state, R_0 , is expected to be proportional to $1/d$ (Equation (10)). For an electrical characterization of the sensitive layer, complex impedance plots of the samples with sensitive LNT layers of 30 to 150 μm were taken. The electrical properties of all investigated sensor samples between 10 Hz and 20 MHz can be described by an $R||C$ equivalent circuit. Figure 5(a) shows exemplarily Nyquist plots of samples with layers of 30, 60, and 90 μm . The data points measured at 1 kHz are marked. Fitting the spectra by an $R||C$ model, the values of R_0 were obtained and are plotted as a function of $1/d$ in Figure 5(b). R_0 increases with decreasing thickness, although no exact $1/d$ -dependency occurs. The resistances of the samples with the thinnest layers (30 μm) are especially high, resulting in deviations from the expected $1/d$ -behavior (Equation (10)). This may be caused by the loose packing of the catalyst particles in the coating and by inaccuracies in the thickness estimation due to the film unevenness. Furthermore, the simple model depicted in Figure 3(a) that leads to Equation (10) is only valid if the layers are by far thinner than the distance between the IDE fingers ($d \ll l'$). This was confirmed in [28] by modeling the electrical flux lines in a system of a highly resistive substrate, metallic IDEs, and a resistive sensitive layer covering the IDEs. Since the distance between the electrodes of the applied IDE samples is 100 μm , it is

assumed that in samples with coating of 100 μm and above there are less flux lines in the outer LNT material. Therefore, the outer parts of the LNT layer do not or only slightly contribute to the overall resistance. As a result, these thicker films may no longer exhibit the $R_0 \propto 1/d$ behavior.

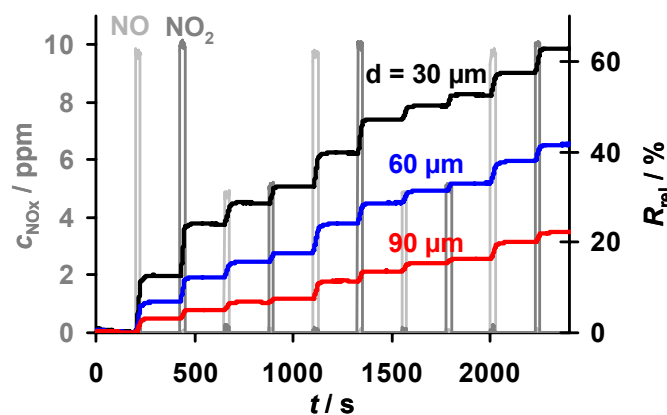
Figure 5. Effect of the thickness of the sensitive layer on the electrical properties in the unloaded state: (a) Complex impedance plots of samples with 30 μm , 60 μm , and 90 μm (data points at 1 kHz are marked); (b) base resistance, R_0 , as a function of the inverse thickness, $1/d$.



5.3. Direct Accumulative Amount Detection

A cyclic test program to investigate the accumulating sensing properties of the samples with various thicknesses in low levels of NO_x (here 10 ppm and less), especially the holding capability in the absence of NO_x , is given in Figure 6. Also shown is a comparison of the sensor responses, R_{rel} , towards NO and NO_2 . The samples with layers from 30 to 90 μm were exposed to alternating NO and NO_2 steps of 25 s with concentrations of 5 and 10 ppm interrupted by NO_x pauses of 200 s. Due to the lower resistivity of the nitrate compared to the carbonate form of the storage material, the resistance decreased during NO_x loading, yielding an increase in R_{rel} [10,13]. For all samples in Figure 6, R_{rel} increases linearly at constant NO_x concentration, with an almost equal response to NO and NO_2 , while R_{rel} remains constant in 0 ppm NO_x . It is evident that the sensors are less sensitive to NO_x the thicker the storage layers are, albeit the samples are exposed to the same NO_x profile. The constancy of R_{rel} during the 200 s intervals without NO_x reveals that all sensitive layers are able to keep the stepwise accumulated NO_x molecules - even in the absence of NO_x . This indicates that the storage capacities of the samples with various thicknesses are not nearing saturation and that the formed nitrates are highly stable in the applied conditions enabling accumulating NO_x sensing. Hence, all applied samples with various thicknesses provide accumulating NO_x sensing properties.

Figure 6. Accumulating sensor responses, R_{rel} , of the samples with various thicknesses increasing stepwise during cyclic exposure to 5 or 10 ppm NO (light grey line) or NO₂ (dark grey line) for 25 s each alternating with 0 ppm NO_x for 200 s.

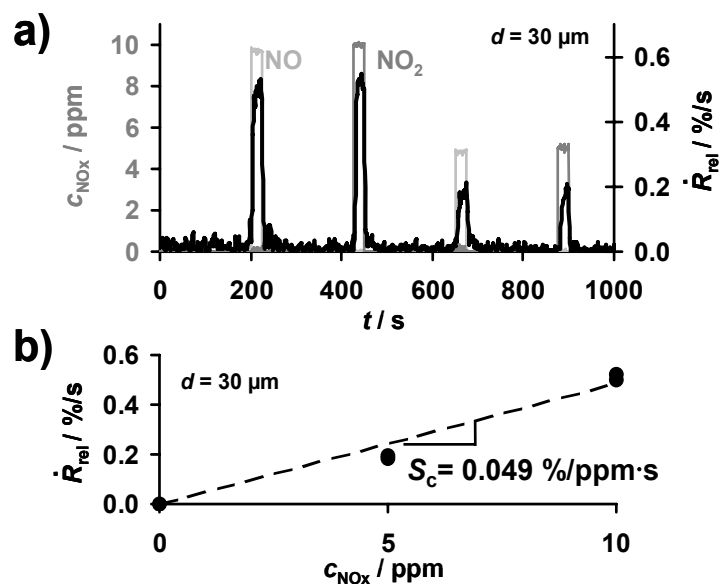


A more detailed analysis of the dependency of the sensitivity, the linear measurement range and the sensor response time on the thickness of the sensitive layer is given in the next sections.

5.4. Concentration Detection by the Signal Derivative

The progressive accumulation of NO_x molecules in the sensitive layer in the presence of NO_x enables the direct detection of the total NO_x amount. As sketched in Figure 2, in the case of a constant flow rate, the time-based signal derivative, \dot{R}_{rel} according to Equation (3), of the ideal accumulating sensor in the low loaded state can be applied to obtain information about the actual NO_x concentration, c_{NO_x} . To compare accumulating-type sensors with conventional gas sensors, one has to analyze the concentration sensitivity S_c , *i.e.*, the derivative $S_c = d\dot{R}_{rel}/dc$ according to Equation (5). Exemplarily, the corresponding data of the signal derivative \dot{R}_{rel} of the sample coated with a 30 μm storage layer are plotted in Figure 7(a). During the first four NO_x periods, \dot{R}_{rel} reflects the curve of c_{NO_x} being the sum of c_{NO} and c_{NO_2} allowing for determining the actual NO_x concentration. The corresponding characteristic line for the concentration detection correlating \dot{R}_{rel} and c_{NO_x} is given in Figure 7(b). \dot{R}_{rel} increases with an increased NO_x concentration in the gas. Hence, the NO_x sensitivity, S_c , of the 30 μm sample can be calculated from Equation (5) and was found to be 0.049%/ppm·s. This means that the resistance decreases by 0.049%/s upon exposure to 1 ppm NO_x. The analysis of the sensor response times for the concentration detection by \dot{R}_{rel} in dependency of the thickness of the sensitive layer will be discussed in detail in Sections 5 and 6. From \dot{R}_{rel} in Figure 7, one obtains a sensor response and recovery time of about 5 to 8 s, which is in the range of the gas exchange time of the setup. Figure 7 demonstrates that besides detecting directly the total NO_x amount, the signal derivative of the accumulating NO_x sensor allows NO_x concentration monitoring with a high sensitivity and a fast sensor response.

Figure 7. Signal derivative, \dot{R}_{rel} , of the 30 μm sample during cyclic exposure to NO and NO₂: (a) \dot{R}_{rel} of the 30 μm sample corresponding with the actual NO_x concentration, c_{NO_x} ; (b) resulting correlation between \dot{R}_{rel} and c_{NO_x} .



5.5. The Effect of the Thickness on the Sensitivity

According to the simplified model that is based on the assumption that a thin nitrate layer forms at the surface of the sensitive storage layer upon NO_x exposure, as shown in Figure 3, and the resulting Equation (13), both sensitivities, S_A and S_c , should increase with $1/d$. The characteristic lines, correlating R_{rel} with the total NO_x amount, A , extracted from the cyclic measurement data presented in Figure 6 are shown in Figure 8(a). For each sample, the data points of R_{rel} measured at the end of each NO_x step form straight lines through the origin up to a sensor response of about 30%, independent of the NO_x concentration or the type of NO_x (NO or NO₂). Comparing the characteristic lines for the amount detection of the samples with different thicknesses in Figure 8(a), it becomes clear that S_A decreases when the sensitive layer gets thicker. To evaluate the thickness effect in detail, S_A is plotted as a function of $1/d$ in Figure 8(b). S_A increases linearly with $1/d$ with small deviations in the case of layers being 90 μm or thicker ($1/d \leq 0.011 \mu\text{m}^{-1}$).

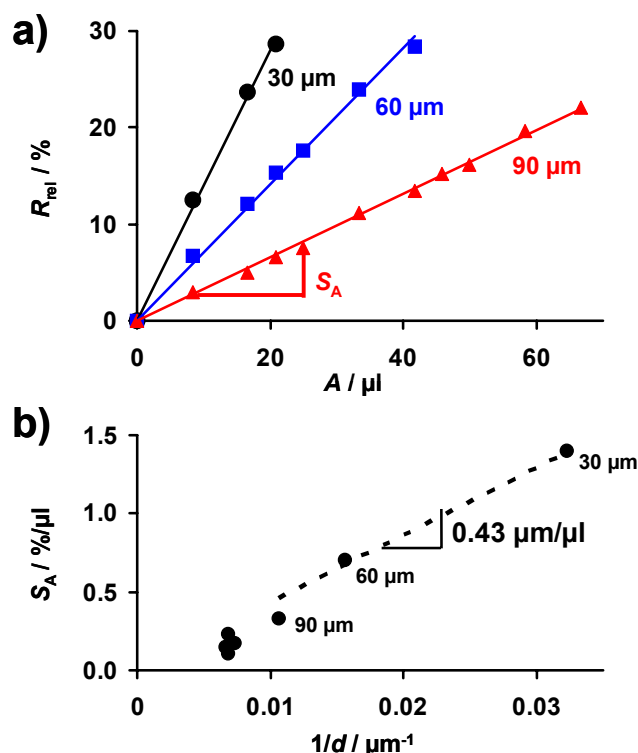
From the concentration related sensitivity $S_c \approx 0.049\%/ppm \cdot s$ of the 30 μm sample determined from Figure 7(b) and the applied gas flow of $\dot{V} = 2 \text{ L/min} = 0.033 \text{ L/s}$, the sensitivity S_A can be calculated. Applying the relationship between S_A and S_c described by Equation (7) one obtains $S_A \approx 1.48\%/μ\text{L}$, which agrees with the value shown in Figure 8(b) for the 30 μm sample. This good agreement verifies that validity of the correlation between S_A and S_c (Equation (7)).

These results verify the simplified model as illustrated in Figure 3 and demonstrate that the thickness of the accumulating NO_x storage layer can be used as an effective tool to adapt the sensor sensitivity to the application requirements.

According to Equation (14) a linear correlation between S_A and $1/d$ with a proportionality factor of $\rho_0/\rho_{\text{NO}_x} \cdot d(d_{\text{NO}_x})/dA$ can be expected from the simplified model. Hence, applying the slope of the correlation in Figure 8(b), $dS/d(1/d)$, the thickness of the formed nitrate layer, d_{NO_x} , dependent on the exposed amount of NO_x can be estimated. Since the resistivity of the samples was found to decrease by

at least one order upon saturation in NO_x (result not shown here), $\rho_0/\rho_{\text{NO}_x} \approx 10$ is assumed as a minimal value. With the slope $dS/d(1/d)$ being $0.43 \mu\text{m}/\mu\text{L}$ (dotted line in Figure 8(b) for samples $<100 \mu\text{m}$), d_{NO_x} increases by less than about 43 nm per $\mu\text{L NO}_x$ in the gas phase.

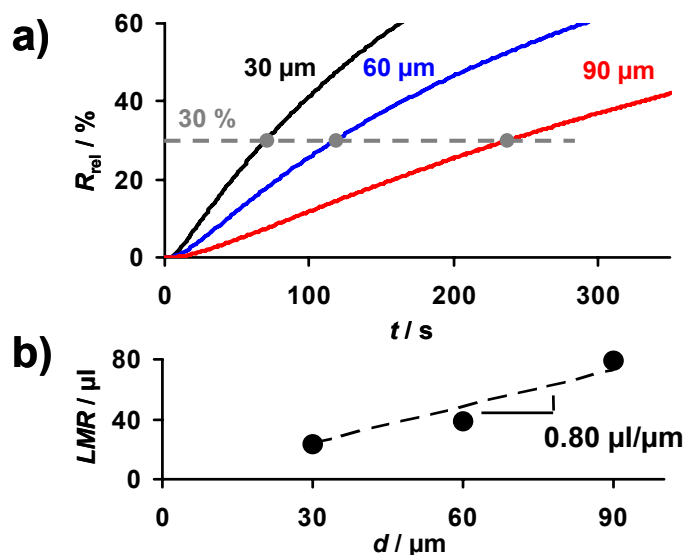
Figure 8. Layer thickness influence on the sensitivity: (a) Comparison of the characteristic lines for different coating thicknesses; (b) the resulting values of the amount-sensitivity, S_A , as a function of $1/d$.



5.6. Variations of the Linear Measurement Range

As sketched in Figure 2, the linear measurement range, LMR , is defined as the amount of NO_x that can be detected when a linear correlation between R_{rel} and A exists. The LMR ends when saturation effects occur and the sensitivities S_A and S_c decrease. Therefore, besides the sensitivity and the sensor response time, the LMR is an important feature of the accumulating-type sensor. The effect of the sensitive layer thickness on the LMR is addressed in Figure 9. In the presence of 10 ppm NO_x (consisting of 5 ppm NO and 5 ppm NO_2) in a lean gas mixture, R_{rel} of all samples increases continuously with time (Figure 9(a)). In accordance to Equation (14), the sensitivity is higher in the case of thinner sensitive storage layers. From Figure 9(a) it seems that, independent on the sensitive layer thickness, the LMR ends at about $R_{\text{rel}} = 30\%$. This results in an increase of the LMR -amount with the layer thickness as shown in Figure 9(b). The slope in Figure 9(b) indicates that $0.80 \mu\text{L NO}_x$ can be detected linearly per $\mu\text{m LNT}$ layer deposited on the sensor.

Figure 9. The effect of the thickness on the linear measurement range, *LMR*: (a) R_{rel} increases linearly in the presence of 5 ppm NO and 5 ppm NO₂ up to about 30%, (b) *LMR* as a function of d .



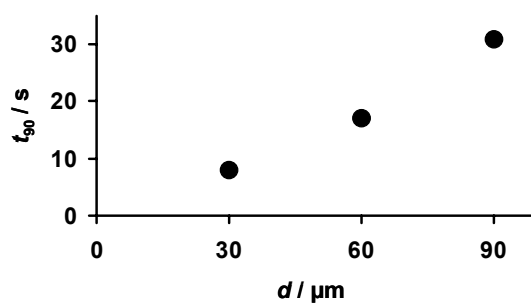
In Section 5.5, it was calculated that the thickness of the nitrate fraction of the sensitive layer increases by about 43 nm/ μL . This value can be combined with the dependency of the *LMR* on d of 0.80 $\mu L / \mu m$ from Figure 9(b). One obtains that if reaching the end of the linear measurement range upon NO_x exposure 43 nm/ μL · 0.80 $\mu L / \mu m$ = 34 nm nitrate is formed per μm LNT material. In other words, independent of the LNT thickness only about 3% of the sensitive material is converted to nitrate in the case of NO_x storage in the linear measurement range. This estimated nitrate fraction of the sensitive layer is much less than the values reported for the storage sites utilization of LNT catalysts of maximal 20 to 40% upon saturation [23–25]. This difference indicates that the end of the linear measurement range of the accumulating NO_x sensor might be limited rather by the non-linear relation between resistivity change and NO_x loading than by the storage capacity of the LNT material.

5.7. Evaluation of the Sensor Response Time

With the accumulating NO_x sensor the amount of NO_x is detected by looking on the changes in the electrical properties and not on the equilibrium values like with conventional gas sensors. Hence, no sensor response time of R_{rel} can be defined in the classical way. Instead one has to apply the timely derivative, \dot{R}_{rel} , which is a function of the concentration and therefore corresponds to the sensor signal of conventional gas sensors. From the measured data of the samples in 10 ppm NO_x, the sensor response time of the slope \dot{R}_{rel} was analyzed. Therefore, the time to reach 90% of the maximum value of \dot{R}_{rel} , t_{90} , is compared for the samples with different coating thicknesses. Figure 10 shows that t_{90} increases with d . While t_{90} of the sample with a 30 μm storage layer is about 7 s, it is in the range of 30 s in the case of the 90 μm sample. In the case of very thin coatings the sensor response is limited by the gas exchange of the test bench, which is in the range of 7 s. For very thick coatings ($d \approx l$), NO_x storage occurs in a region far away from the electrodes. Due to the increasingly weaker electrical field lines, NO_x uptake in this region of the LNT layer is most probably not reflected properly by R_{rel} and

\dot{R}_{rel} . Additionally, it is expected that the accessibility of the storage sites is dependent on the LNT thickness as with progressive NO_x loading upcoming NO_x molecules need to diffuse into the catalyst material to reach unoccupied storage sites [26,27,31]. The analysis of the sensitivity and the sensor response time in Figures 8 and 10 clarifies that for a highly sensitive and fast low level detection of NO_x , accumulating NO_x sensors with a thin sensitive layer are preferable.

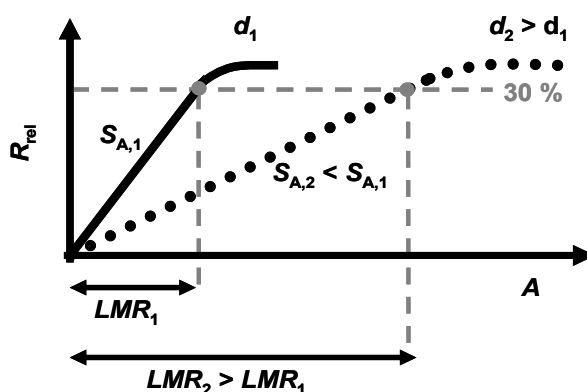
Figure 10. Analysis of the sensor response time, t_{90} , of \dot{R}_{rel} in 10 ppm NO_x as a function of the thickness d .



6. Conclusions

The intent of this study was to investigate the influence of the sensitive layer thickness on the sensing properties of the accumulating NO_x sensor. In several NO_x loading experiments it was demonstrated that the general accumulating NO_x amount sensing properties seem not to be affected by the thickness of the sensitive layer in the studied range (*i.e.*, the increase of the sensor signal in the presence of NO_x due to NO_x accumulation, the correlation between the slope and the NO_x concentration, and the constancy of the sensor signal in the NO_x absence due to the strength of sorption). The linearity of the sensor signal, R_{rel} , with the total NO_x amount enables the detection of the actual NO_x concentration by \dot{R}_{rel} with all applied samples.

Figure 11. Illustration of the effect of the thickness of the sensitive layer ($d_1 < d_2$) on the sensitivity, S_A , and the linear measurement range, LMR , with the end of the linear measurement range being at 30% signal change.



However, like the base resistance, the sensitivity to NO_x is inversely proportional to the film thickness d . This agrees with a simple model concerning nitrate formation at the surface of the sensitive layer. It was demonstrated that NO_x can be detected linearly until the sensor resistances

reaches about 30%. This limit was found to be independent on the thickness of the sensitive layer. This controversial effect of the sensitive layer thickness on the sensitivity, S_A (and also on S_C), and on the linear measurement range, LMR , is illustrated in Figure 11 for two samples with two different thicknesses, d_2 (dark grey line) being higher than d_1 (light grey line). While S_1 is higher than S_2 , the resulting LMR_2 is larger than LMR_1 . More particularly, LMR increases with d allowing for a measurement range adaption depending on the requirements of the application conditions. However, there is a trade-off between a large linear measurement range and a high sensitivity.

The presented measurement results also point out that the timely sensor response characteristic depends on the thickness of the storage material. In the case of very thin layers (30 μm) the sensor response time corresponds to the gas exchange time of the gas flow stand, whereas the sensor signal becomes slower as the thickness increases. An estimation based on the presented simplified model of the sensor setup reveals that, independently on the thickness of the LNT material only a small fraction of the sensitive layer—probably about 3%—is involved in the NO_x storage process as the accumulating sensor is operated in the linear measurement range.

Acknowledgements

The authors gratefully acknowledge the LNT material preparation by Shadab Mulla, Todd H. Ballinger, Hai-Ying Chen (Johnson Matthey) and the SEM analysis by Angelika Mergner (Lehrstuhl Funktionsmaterialien). Ralf Moos thanks the German Research Foundation (DFG) for supporting this work under grant number MO 1060/15-1. This publication was funded by the German Research Foundation (DFG) and the University of Bayreuth in the funding program “Open Access Publishing”.

References

1. Afzal, A.; Cioffi, N.; Sabbatini, L.; Torsi, L. NO_x sensors based on semiconducting metal oxide nanostructures: Progress and perspectives. *Sens. Actuators B Chem.* **2012**, *171–172*, 25–42.
2. Kim, Y.-W.; van Nieuwstadt, M. *Threshold Monitoring of Urea SCR Systems*; SAE Technical Paper 2006-01-3548; SAE 2006 Commercial Vehicle Engineering Congress & Exhibition: Rosemont, IL, USA, October 2006.
3. Sasaki, H.; Scholl, D.; Parsons, M.; Inagaki, H.; Shiotani, K.; Visser, J.; Zawacki, G.; Kawai, T.; Teramoto, S.; Kubinski, D. *Development of an $\text{Al}_2\text{O}_3/\text{ZrO}_2$ -Composite High-Accuracy NO_x Sensor*; SAE Technical Paper 2010-01-0041; SAE 2010 World Congress & Exhibition: Detroit, MI, USA, April 2010.
4. *Directive 2008/50/EC of the European Parliament and of the Council of 21 May 2008 on Ambient Air Quality and Cleaner Air for Europe*; Official Journal of the European Union, 2008; L152/1.
5. Alkemade, U.G.; Schumann, B. Engines and exhaust after treatment systems for future automotive applications. *Solid State Ionics* **2006**, *177*, 2291–2296.
6. Twigg, M.V. Progress and future challenges in controlling automotive exhaust gas emissions. *Appl. Catal. B Environ.* **2007**, *70*, 2–15.
7. Padilla, M.; Perera, A.; Montoliu, I.; Chaudry, A.; Persaud, K.; Marco, S. Drift compensation of gas sensor array data by orthogonal signal correction. *Chemometr. Intell. Lab. Syst.* **2010**, *100*, 28–35.

8. Sickles, J.E.; Grohse, P.M.; Hodson, L.L.; Salmons, C.A.; Cox, K.W.; Turner, A.R.; Estes, E.D. Development of a method for the sampling and analysis of sulfur dioxide and nitrogen dioxide from ambient air. *Anal. Chem.* **1990**, *62*, 338–346.
9. Varshney, C.K.; Singh, A.P. Passive samplers for NO_x monitoring: A critical review. *Environmentalist* **2003**, *23*, 127–136.
10. Groß, A.; Beulertz, G.; Marr, I.; Kubinski, D.J.; Visser, J.H.; Moos, R. Dual mode NO_x sensor: Measuring both the accumulated amount and instantaneous level at low concentrations. *Sensors* **2012**, *12*, 2831–2850.
11. Beulertz, G.; Groß, A.; Moos, R.; Kubinski, D.J.; Visser, J.H. Determining the total amount of NO_x in a gas stream—Advances in the accumulating gas sensor principle. *Sens. Actuators B Chem.* **2012**, doi:10.1016/j.snb.2012.02.017.
12. Moos, R.; Wedemann, M.; Spörl, M.; Reiß, S.; Fischerauer, G. Direct catalyst monitoring by electrical means: An overview on promising novel principles. *Top. Catal.* **2009**, *52*, 2035–2040.
13. Fremerey, P.; Reiß, S.; Geupel, A.; Fischerauer, G.; Moos, R. Determination of the NO_x loading of an automotive lean NO_x trap by directly monitoring the electrical properties of the catalyst material itself. *Sensors* **2011**, *11*, 8261–8280.
14. Moos, R.; Zimmermann, C.; Birkhofer, T.; Knezevic, A.; Plog, C.; Busch, M.R.; Ried, T. *Sensor for Directly Determining the State of a No_x Storage Catalyst*; SAE Technical Paper 2008-01-0447; SAE World Congress & Exhibition: Detroit, MI, USA, April 2008; doi:10.4271/2008-01-0447.
15. Groß, A.; Bishop, S.R.; Yang, D.J.; Tuller, H.L.; Moos, R. The electrical properties of NO_x-storing carbonates during NO_x exposure. *Solid State Ionics* **2012**, doi:10.1016/j.ssi.2012.05.009.
16. Morrison, S.R.; Madou, M.J. *Chemical Sensing with Solid State Devices*; Academic Press Inc.: London, UK, May 1989.
17. Epling, W.S.; Campbell, L.E.; Yezerets, A.; Currier, N.W.; Parks, J.E., II. Overview of the fundamental reactions and degradation mechanism of NO_x storage/reduction catalysts. *Catal. Rev.* **2004**, *46*, 163–245.
18. Roy, S.; Baiker, A. NO_x storage-reduction catalysis: From mechanism and materials properties to storage-reduction performance. *Chem. Rev.* **2009**, *109*, 4054–4091.
19. Liu, G.; Gao, P.-X. A review of NO_x storage/reduction catalysts: Mechanism, materials and degradation studies. *Catal. Sci. Technol.* **2011**, *1*, 552–568.
20. Lesage, T.; Saussey, J.; Malo, S.; Hervieu, M.; Hedouin, C.; Blanchard, G.; Daturi, M. Operando FTIR study of NO_x storage over a Pt/K/Mn/Al₂O₃-CeO₂ catalyst. *Appl. Catal. B Environ.* **2007**, *72*, 166–177.
21. Geupel, A.; Schönauer, D.; Röder-Roith, U.; Kubinski, D.J.; Mulla, S.; Ballinger, T.H.; Chen, H.-Y.; Visser, J.H.; Moos, R. Integrating nitrogen oxide sensor: A novel concept for measuring low concentrations in the exhaust gas. *Sens. Actuators B Chem.* **2010**, *145*, 756–761.
22. Geupel, A.; Kubinski, D.J.; Mulla, S.; Ballinger, T.H.; Chen, H.-Y.; Visser, J.H.; Moos, R. Integrating NO_x sensor for automotive exhausts—A novel concept. *Sens. Lett.* **2011**, *9*, 311–315.
23. Castoldi, L.; Lietti, L.; Forzatti, P.; Morandi, S.; Ghiotti, G.; Vindigni, F. The NO_x storage-reduction on Pt-K/Al₂O₃ lean NO_x trap catalyst. *J. Catal.* **2010**, *276*, 335–350.

24. Muncrief, R.L.; Khanna, P.; Kabin, K.S.; Harold, M.P. Mechanistic and kinetic studies of NO_x storage and reduction on Pt/BaO/Al₂O₃. *Catal. Today* **2004**, *98*, 393–402.
25. Scholz, C.M.L.; Gangwal, V.R.; de Croon, M.H.J.M.; Schouten, J.C. Influence of CO₂ and H₂O on NO_x storage and reduction on a Pt–Ba/γ-Al₂O₃ catalyst. *Appl. Catal. B Environ.* **2007**, *71*, 143–150.
26. Tuttlies, U.; Schmeißer, V.; Eigenberger, G. A mechanistic simulation model for NO_x storage catalyst dynamics. *Chem. Eng. Sci.* **2004**, *59*, 4731–4738.
27. Olsson, L.; Blint, R.J.; Fridell, E. Global kinetic model for lean NO_x traps, *Ind. Eng. Chem. Res.* **2005**, *44*, 3021–3032.
28. Hagen, G. Impedimetric Zeolite-Based Gas Sensors. Ph.D. Dissertation, Universität Bayreuth, Bayreuth, Germany, 2009.
29. Schönauer, D.; Moos, R. Detection of water droplets on exhaust gas sensors. *Sens. Actuators B Chem.* **2010**, *148*, 624–629.
30. Chen, H.-Y.; Mulla, S.; Ballinger, T.H. No_x Storage Materials for Sensor Applications, U.S. Patent 20,100,146,935, 17 June 2010.
31. Rettig, F.; Moos, R.; Plog, C. Sulfur adsorber for thick-film exhaust gas sensors. *Sens. Actuators B Chem.* **2003**, *93*, 36–42.

© 2012 by the authors; licensee MDPI, Basel, Switzerland. This article is an open access article distributed under the terms and conditions of the Creative Commons Attribution license (<http://creativecommons.org/licenses/by/3.0/>).